Anura3D

MPM Research Community

Numerical simulation of a free fall penetrometer deployment using the Material Point Method

Luis, Zambrano-Cruzatty[1*], Alba, Yerro[1]

[1]Department of Civil and Environmental Engineering, Virginia Polytechnic Institute and State University, Blacksburg, VA, USA

[*] E-mail: luisez@vt.edu

ABSTRACT

This paper proposes a numerical framework to model the deployment of a Free Fall Penetrometer (FFP) device in dry sands using the Material Point Method (MPM). Seabed characterization is required to assess a number of geotechnical problems in the nearshore and offshore areas, and FFP deployment is becoming a popular method to characterize shallow sediments. A moving mesh technique is used to ensure the accurate geometry of the FFP device throughout the calculation and the soil-FFP interaction is modelled with a frictional contact algorithm. The FFP device is simulated as a rigid body, which enhances the performance of the computation and reduces its computational cost. Numerical results are compared to experimental data, and are very promising.

KEY WORDS: Free fall penetrometer; cone testing; impact penetration; sediment characterization; moving mesh.

INTRODUCTION

Geotechnical engineering activities in the nearshore and offshore zones are increasing due to population growth in the coastal areas, offshore wind farming projects, offshore mining industry activities, among others. Seabed characterization is required to assess different geotechnical problems such as determining the bearing capacity of soils for submarine piping. However, soil characterization in the sea environment is usually prohibitively expensive, slow, and in some cases logistically impossible (e.g., high energetic wave conditions). In this context, Free Fall Penetrometer (FFP) testing is becoming a popular method to characterize shallow sediments because it is a fast, cheap, and versatile test (Stark et al., 2014). FFP testing consists of a torpedo-like device with embedded sensors that free fall through air or water impacting the soil at terminal velocities between 3-6 m/s (Albatal et al., 2017). After the impact, the FFP penetrates the sediment until the resistance forces in the soil exceed the driving forces on the FFP, recording the changes in acceleration and pore pressures. Despite the increasing popularity of FFP testing, the data interpretation still relies on empirical correlations to determine the sediment properties due to complexities associated to fast impact problems (Moavenian et al., 2016; Nazem et al., 2012). The development of reliable numerical models is essential to obtain a more comprehensive and accurate understanding of the problem.

The modelling of FFP testing is complex because it has to address FFP device-soil interaction, transient velocities, large soil deformation, hydro-mechanical coupling between soil skeleton and pore water pressures, strain-rate strength dependency among others (Nazem et al., 2012; Moavenian et al., 2016; Sabetamal et al., 2018). Aubeny and Shi (2006) used a quasi-static FEM analysis to simulate the FFP in undrained clay. Although the results were consistent with field data, the dynamic effects behind FFP penetration were not fully captured by this approach. Nazem et al. (2012) and Moavenian et al. (2016) performed a dynamic simulation using the Lagrangian-Eulerian FEM (ALE), but these simulations require remeshing techniques that are heavily demanding on computational resources. Recently, Sabetamal et al. (2018) performed a simulation of FFP penetration using the ALE effective stress analysis to study the pore pressure development during the penetration in clays. These examples are brought into discussion to illustrate two main points: 1) numerical techniques taken into account to simulate impact penetration problems are computationally expensive; and 2) there is a lack of simulations of FFP penetration in coarse material.

MPM is a suitable alternative to model FFP testing since it is capable of handling high impact velocities, large deformations without mesh tangling, soil-structure interaction, and hydro-mechanical coupling using two-phase formulations. Examples of previous MPM penetration problems in geotechnics are the following: Al-Kafaji (2013) modeled the penetration of piezocones, spheres, and torpedo anchors; Ceccato et al. (2016) presented CPT penetration; and Phuong et al. (2016) modeled pile installation.

In this study, the effectiveness of the MPM for simulating fast penetration is investigated. In particular, a framework capable to model the FFP deployment on dry sand is presented. A moving mesh technique attached to the FFP structure is considered to ensure a well-defined FFP geometry throughout the calculation. The interaction between soil and FFP is modelled by means of a frictional contact algorithm, and the effect of different contact shear strengths is evaluated. The compressibility of the FFP device is also discussed and a rigid body algorithm is proposed to reduce computational resources. Finally, the numerical results are compared with experimental data. This analysis is performed with the internal version of the Anura3D MPM software.

EXPERIMENTAL SETUP

A set of experiments have been carried out at Virginia Tech in which a Bluedrop FFP device (Figure 1a) was deployed in a modified calibration chamber filled with dry sand. The chamber was cylindrical, with 0.8 m of diameter and 0.4 m of height (Figure 1b). The FFP device was dropped at a controlled height (h_d) to regulate the impact velocity, and four accelerometers installed on the FFP collected deceleration measurements during penetration (Albatal, 2018). Figure 1b illustrates the setup of the laboratory experiments and the Bluedrop FFP original design.

The sand parameters were investigated by Albatal (2018) who developed a correlation for the peak friction angle and the relative density of the sand using a triaxial vacuum test. It was found that the sand relative density ranges between 15 % and 17% with a mean unit weight of 15.1 kN/m^3, and the sand friction angle was estimated as $\phi'=40°$.

NUMERICAL MODEL

The geometry of the model is defined taking advantage of the symmetry of the experimental tests, hence a 20° slice of 1.1 m height and 0.4 m radius is considered (Figure 2). The dimensions are consistent with the physical experiment setup. The FFP geometry consists of a 60° cone tip, and the outer edge has been slightly smoothed with respect to the original design to reduce numerical singularities. The cone is placed in immediate contact with the soil and based on physical experiments, a 5.6 m/s initial impact velocity is assigned to the FFP. The FFP body mass is 7.71 kg.
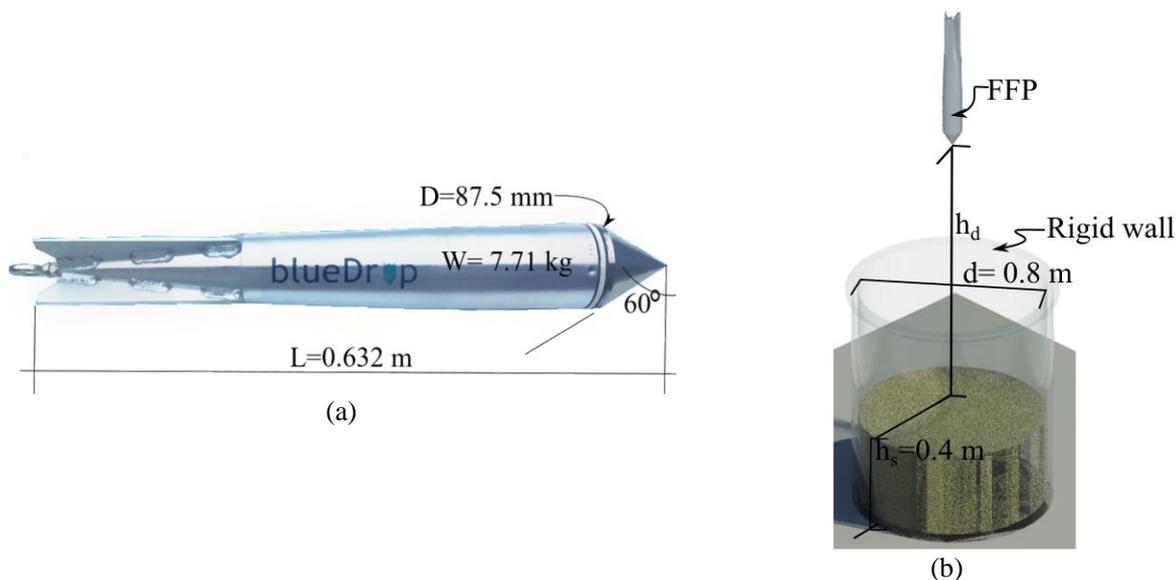

Figure 1 (a) Blue Drop FFP device. After Blue C Designs Inc. (www.bluecdesigns.com) (b) FFP experimental setup sketch

The Mohr-Coulomb failure criterion is selected to simulate the constitutive behaviour of the sand, with an effective friction angle of ϕ'=40°. Cohesion and dilatancy are assumed null. The Young's modulus is calculated from the triaxial data provided in Albatal (2018), which is found to be 5,000 kPa for a sand specimen with 15 % of relative density. The Poisson ratio is assumed to be 0.33.

A fully dynamic MPM formulation is considered and artificial damping is not treated. A tetrahedral mesh is used to discretize the model in which the minimum element size, assigned around the cone, is 1 cm. This distribution was found to optimize computational resources while giving accurate discretization of the FFP-soil contact surface. Ten material points are initially distributed in the elements representing the soil, while one material point is considered in the FFP elements. The total number of material points is 326,592. The fixities applied to the background mesh are indicated in Figure 2 and ensure axisymmetric conditions; the bottom is fully fixed while other boundaries only allow free vertical displacements. A moving mesh technique is used to ensure that the FFP geometry remains well-defined throughout the penetration. This technique consists of subdividing the background computational mesh into a moving mesh and a compressing mesh. While the moving part moves following a reference material, in this case, the FFP; the remaining part compresses at the same rate (Figure 2). In this manner, the material points from the FFP stay inside their original elements throughout the simulation while keeping a well-defined contact surface (Ceccato et al., 2016; Phuong et al., 2016).
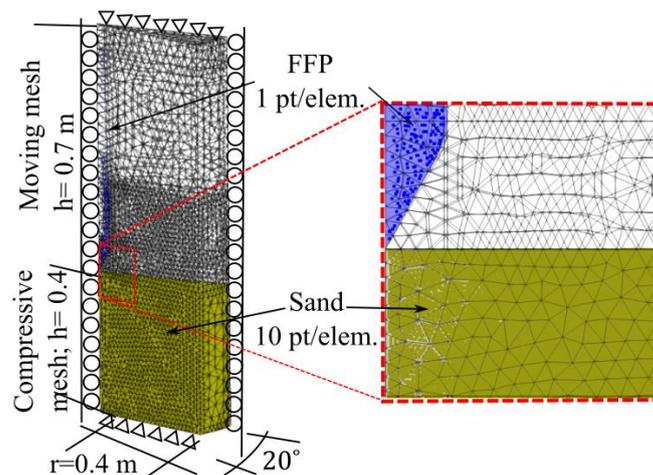

Figure 2 Model geometry configuration

FFP-soil contact simulation

Problems in geotechnical engineering involving the interaction of rigid elements and soil are governed by relative slip along the contact surfaces of interaction; this has been recognized for the particular case of cone penetration and impacts penetration by Durgunoglu & Mitchell (1973) and Albatal (2018) respectively. However, MPM inherently handles non-slip contact. Hence, an algorithm capable of allowing slip while preventing interpenetration is taken into account to allow relative slip between surfaces.

The Anura3D software uses the algorithm proposed by Bardenhagen et al. (2000). However, a shortcoming of the Bardenhagen et al. (2000) algorithm appears when, in a contact node, the mass corresponding to one of the materials is very small compared to the masses from other materials in the contact. As a result, the velocity of the first material tends to infinity (Bardenhagen et al., 2001). In this study, this problem arises when a gap between the FFP device and the soil appears as a result of the high impact velocity. On the contact nodes, while the mass from the FFP does not change, the soil mass becomes, in comparison, very small and high unrealistic velocities are observed. Bardenhagen et al. (2001) proposed a solution that consists of evaluating the velocity after the contact algorithm is applied: if the nodal velocity for a particular material is larger than the velocity that would be required to reverse the element geometry, such velocity is scaled down to prevent a hypothetical mesh tangling. The solution proposed by Bardenhagen et al. (2001) has been implemented in this analysis to minimize numerical instabilities, with a scaling factor of 0.75.

Durgunoglu & Mitchell (1973) have shown that the contact friction angle between sand and FFP (δ) can be expressed depending on the soil friction angle as $\delta=\alpha\phi'$, in which α is a factor that depends on the confining

stress, the relative density of the soil, and the roughness of the device's surface. They reported values of α ranging between 0.28 to 0.90, being 0.28 the factor for polished aluminium and 0.9 the factor for sanded aluminium. Based on that, Albatal (2018) estimated that the contact friction angle between the Bluedrop FFP and the sand was approximately $\delta=0.5\,\phi'$. In this study, a parametric analysis has been conducted varying the contact friction angle between 20° to 40°, which corresponds to $\delta=0.5\phi'$ and $\delta=\phi'$ (i.e., fully rough conditions) respectively.

FFP compressibility

Two different approaches are proposed to model the FFP device. The first one assumes that the cone is a linear elastic compressible material, with an elasticity modulus of 20,000 kPa. The second approach considers the FFP as a rigid body (i.e., incompressible).

The procedure adopted to simulate the FFP as a rigid body is described below:
 i) The nodes at the contact are identified, the sum of internal and external forces is balanced with the rate of momentum, and the acceleration of the rigid body is obtained as the ratio between the rate of moment and its total mass as follows:
$$a_{RB} = (m_{RB}g + t_{RB} - \sum_{i=1}^{n} f^i)/m_{RB} \qquad \text{Equation (1)}$$
where a_{RB} is the acceleration vector of the rigid body, m_{RB} is the total mass of the rigid body, g is the gravity acceleration vector, t_{RB} is the external load vector applied to the rigid body (equal to 0 for this study), n is the number of nodes within the contact surface, and f^i is the reaction at the i-th node.
 ii) The acceleration of the rigid body is updated for all the nodes belonging to it:
$$a^i = a_{RB} \qquad \text{Equation (2)}$$
 iii) The nodal velocity is calculated as:
$$v^i = v^i_{\,o} + a^i \Delta t \qquad \text{Equation (3)}$$
with $v^i_{\,o}$ being the velocity at the beginning of each timestep, a^i is the nodal acceleration from the previous step, and Δt is the timestep increment. Note that each node within the rigid body will have the same velocity, which is the rigid body velocity.
 iv) If the contact algorithm is considered, the velocity at the contact nodes may change. Hence, a correction to the nodal accelerations and velocities must be applied. First the corrected rigid body acceleration is computed by:
$$a_{RB,c} = \sum_{i=1}^{N} a^i m^i / m_{RB} \qquad \text{Equation (4)}$$
where $a_{RB,c}$ is the corrected rigid body acceleration, N is the total number of nodes belonging to the rigid body (i.e., FFP), and m^i is the mass associated to the i-th node.
 v) With the corrected acceleration, steps ii) and iii) are repeated.
 vi) The rigid body's acceleration and velocity are written to the corresponding material points and the position is updated.

Note that this approach is not valid for rigid body rotation since the angular momentum is neglected; Additionally, the radial and tangential components of the reaction force are null because the problem is axisymmetric around the FFP axis, and the stresses in the rigid body are not calculated. In this manner, internal deformation is not allowed. Taking into account that the MPM integration is explicit, one advantage of simulating the FFP as a rigid body is that the critical time step is not reduced by the cone's elastic modulus, which is much larger than the soil's elasticity modulus.

RESULTS

Four simulations were carried out combining FFP as a rigid/elastic body, and fully rough/frictional contact. The results regarding penetration depth and reaction at the cone are shown in Figure 3. While the compressibility of the cone (i.e., rigid or elastic) has a minor effect on the penetration depth, the results differ considerably depending on the FFP-soil contact properties (Figure 3a). With the rough contact, the cone penetrates 30% less than with the frictional contact assuming $\delta = 20°$, 14 cm and 20 cm respectively. The evolution of the reaction force at the cone is presented in Figure 3b. In all cases, the reaction increases until a maximum value and then decreases. A second peak with lower amplitude is observed before reaching final stabilization. After some oscillations, the equilibrium is reached, and the reaction is balanced with the self-weight of the FFP.
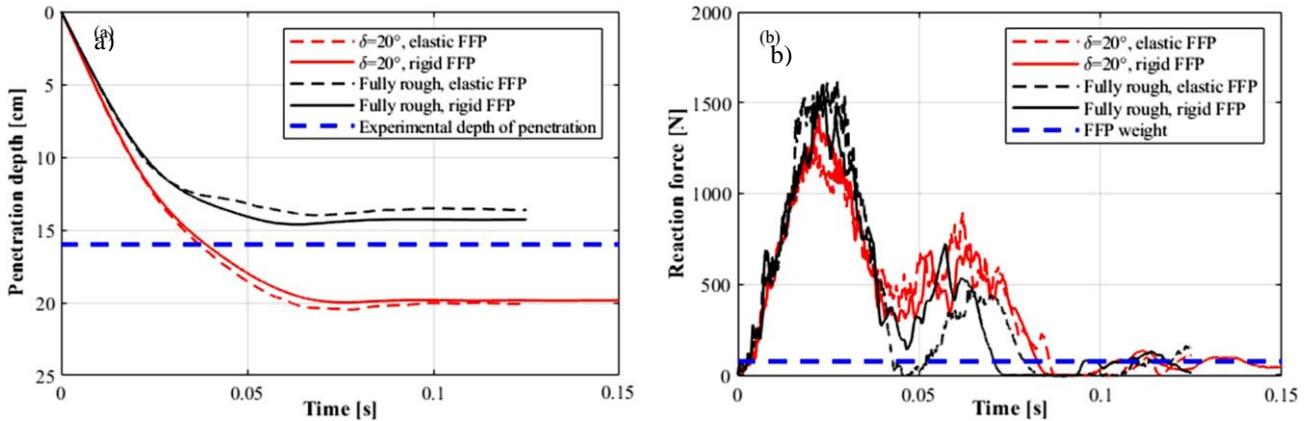
Figure 3 Results obtained for different combinations of FFP simulations with contact and rigid body algorithms.(a) Penetration depth vs. time and (b) vertical reaction vs. time

The maximum reaction occurs when the maximum deceleration is achieved, and its value is higher when the contact is fully rough. Again, the results are similar with regards to changes in FFP compressibility. The advantage of simulating the FFP as a rigid body instead of with the elastic body approach is that the computational time decreased by 37.5% (from 8 to 5 hours with an Intel Core i7 at 2.6 GHz CPU). This can be explained because of: i) the critical time step is increased (i.e., the critical timestep assuming the elastic body approach is 0.539×10^{-5} s, whereas considering the rigid body it increases up to 0.129×10^{-4} s), and ii) the stresses of the material points representing the rigid body are not updated.

Figure 4 shows the evolution of the deviatoric strain at four different times (i.e., t = 0.0 s, 0.02 s, 0.04 s, and 0.08 s) for the case in which the FFP is modelled as a rigid body and the contact friction angle is $\delta = 20°$. At t=0.02 s, the shear strains are essentially located surrounding the cone indicating a local failure. As the cone penetrates, a general bearing capacity failure mechanism is formed (t=0.04 s). The strains tend to be concentrated along a failure surface that propagates until it reaches the sand surface. A passive wedge can be clearly identified in t=0.04 and 0.08 s. It is important to point out that all simulations in this work present failure patterns very similar to the one shown in Figure 4.
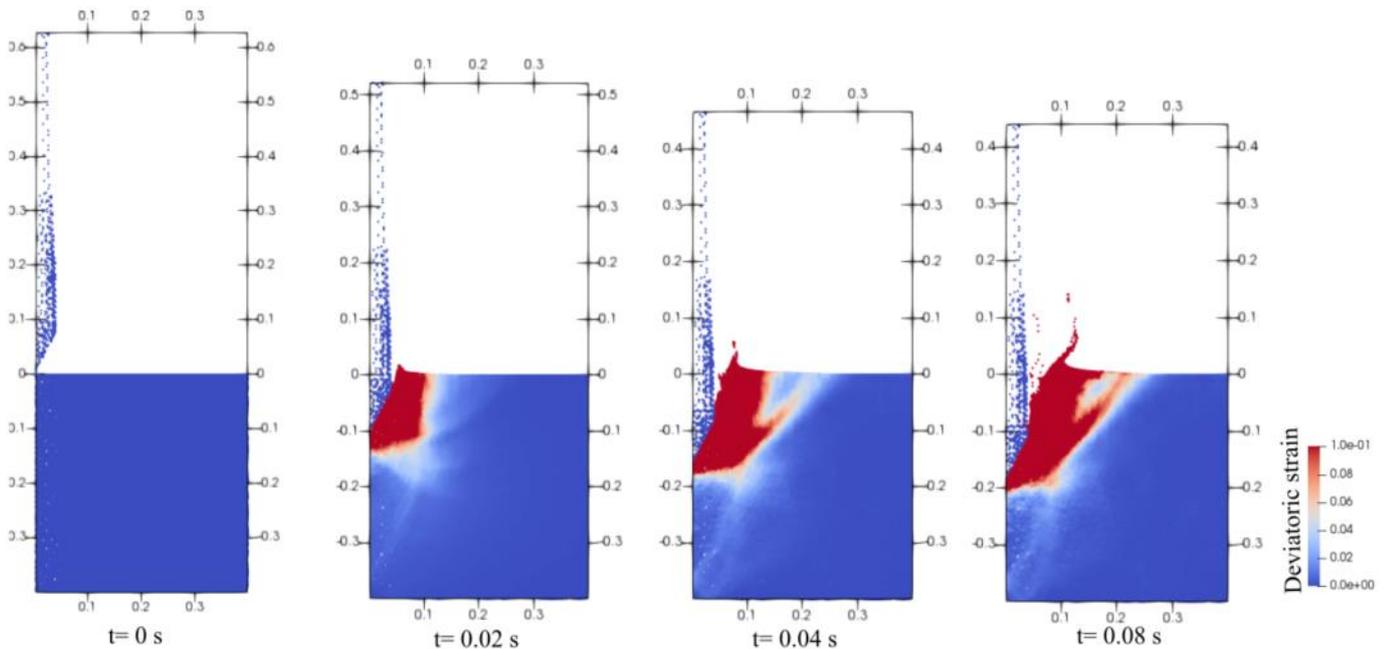

Figure 4 Evolution of the deviatoric strain during the FFP penetration (FFP is assumed as a rigid body and $\delta = 20°$, length dimensions are in [m]).

Taking into account the FFP as a rigid body, a parametric analysis has been performed to study, in more detail, the effect of the contact friction angle (δ). Figure 5 shows the penetration depth vs. time for the simulations with friction angles ranging from 20° to fully rough conditions; the final penetration depth measured in the physical experiment is shown for reference. All simulations present the same penetration rate until t=0.04 s. After that, the penetration rate decreases by different amounts depending on δ until the FFP stabilizes around t=0.06 s. Higher values of δ result in less final penetration, and the numerical case with δ=32° (i.e., δ=0.8ϕ') presents the same penetration measured in the experimental tests.

In Figure 6, the velocity and the deceleration vs. penetration of the FFP for the different friction angles are presented together with experimental data. The behaviour obtained with the MPM results is comparable to the measurements, note that the maximum accelerations obtained from MPM range between 17 g and 23 g, which are similar to the experimental value (i.e., 19.4 g). However, the numerical simulations decelerate slightly faster than experimental results and a secondary peak is observed at the end of the penetration process (Figure 6b), which is also noticeable in the velocity plots (Figure 6a). In terms of velocity and deceleration, the simulation with δ=20° (i.e., δ=0.5ϕ') is the one that fits better the experimental results for most part of the calculation, until the cone reaches a penetration of approximately 12 cm at t=0.025 s.

DISCUSSION

The MPM results are consistent with the experimental data regarding its general behavior and the order of magnitude of the penetration depth, velocity profile, and maximum deceleration. However, at the end of the penetration process, the numerical deceleration presents a secondary peak (Figure 6b) that has an impact on the velocities (Figure 6a). This behaviour can be explained with the late development of the general bearing capacity failure mechanism, in which a wedge becomes kinematically unstable between t=0.02 and t=0.04 s (Figure 4) and the final penetration increases.

The soil response to rapid loading is known to be a function of the strain-rate effects, hence the dilatancy, the peak shear strength, and the elastic properties of the sand tend to increase with the strain-rate (Omidvar, Iskander, & Bless, 2012). In this analysis, the constitutive law taken into account to model the sand behaviour (i.e., Mohr-Coulomb) does not consider these effects. Therefore, this simplification could explain the discrepancy between experimental data and numerical results.

CONCLUSIONS

This work proposes a numerical framework to model the FFP deployment on dry sand. It includes a moving mesh technique and the combination of a contact algorithm and a rigid body formulation. The moving mesh ensures that an accurate FFP geometry throughout the calculation. The contact algorithm proposed by Bardenhagen et al. (2001) is required to simulate the FFP-soil interaction and minimize numerical instabilities. It is found that the modelling of the FFP with a rigid body algorithm improves the performance of the simulation by reducing the computational cost.
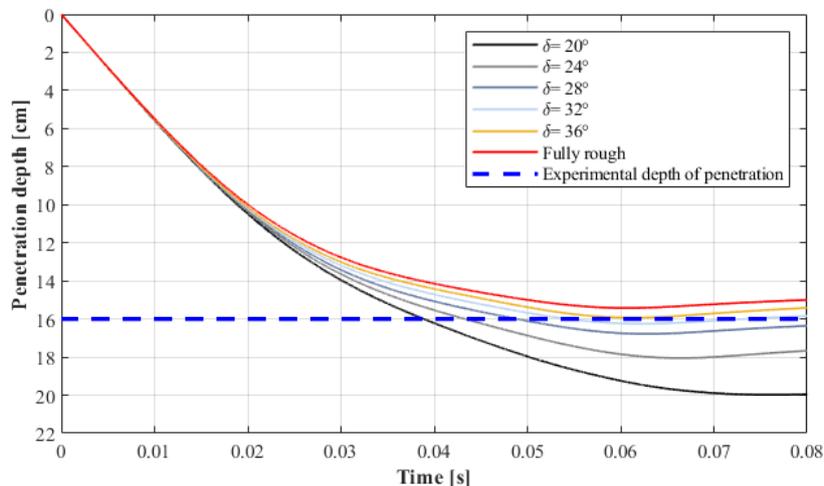

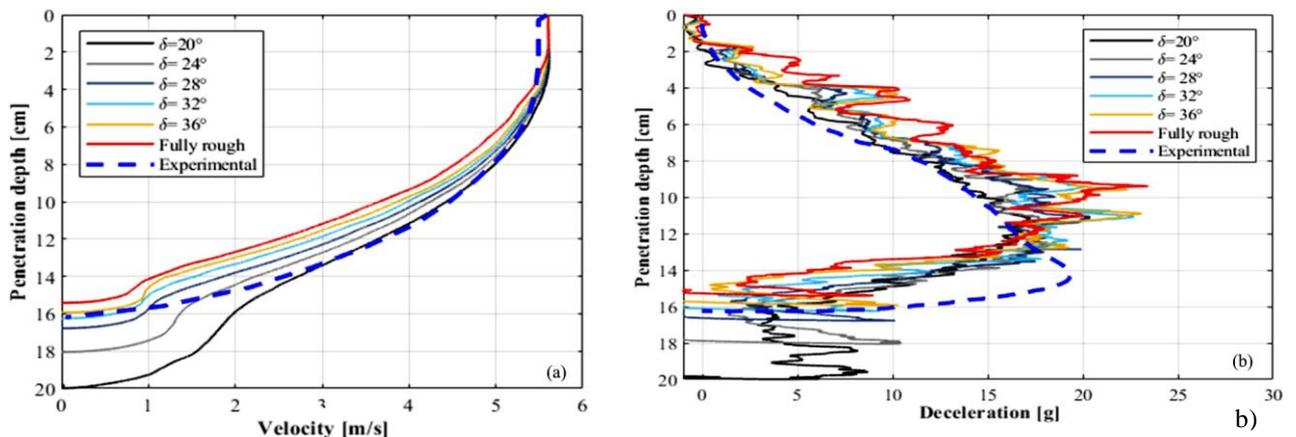Figure 5 Penetration depth vs. time for different contact friction angles

Figure 6 (a) Velocity and (b) deceleration profiles for different contact friction angles. Experimental results are also included

The numerical simulations are compared with experimental data and they are in general agreement. A parametric analysis has been performed to study the effect of the contact friction angle on the results and the range of contact friction angles that best matches the experimental results is 20°-32°, which is consistent with accepted geotechnical literature previously reported (Durgunoglu & Mitchell, 1973). However, some discrepancies have been identified between MPM results and measurements that can be explained because of the constitutive model considered to simulate the sand (i.e., Mohr Coulomb law) does not take into account strain-rate effects due to rapid loading. Therefore, the implementation of a more advanced constitutive model is required to further validate this approach. In any case, the results obtained in this work show that MPM is a promising tool to model fast impact penetration problems.

ACKNOWLEDGEMENTS

REFERENCES

Al-Kafaji, I. K. J. (2013). *Formulation of a Dynamic Material Point Method (MPM) for Geomechanical Problems*. University of Stuttgart, Stuttgart.

Albatal, A. (2018). *Advancement of using portable free fall penetrometers for geotechnical site characterization of energetic sandy nearshore areas*. Virginia Polytechnic Institute and State University, Blacksburg.

Albatal, A., Mcninch, J. E., Wadman, H., & Stark, N. (2017). In-situ geotechnical investigation of nearshore sediments with regard to cross- shore morphodynamics. *Geotechnical Frontiers 2017*, (2011), 398–408.

Aubeny, C. P., & Shi, H. (2006). Interpretation of Impact Penetration Measurements in Soft Clays. *Journal of Geotechnical and Geoenvironmental Engineering*, *132*(6), 770–777.

Bardenhagen, S. G., Brackbill, J. U., & Sulsky, D. (2000). The material-point method for granular materials, (187), 529–541.

Bardenhagen, S. G., Guilkey, J. E., Roessig, K. M., Brackbill, J. U., Witzel, W. M., & Foster, J. C. (2001). An improved contact algorithm for the material point method and application to stress propagation in granular material. *CMES - Computer Modeling in Engineering and Sciences*, *2*(4), 509–522.

Ceccato, F., Beuth, L., Vermeer, P. A., & Simonini, P. (2016). Two-phase Material Point Method applied to the study of cone penetration. *Computers and Geotechnics*, *80*, 440–452.

Durgunoglu, H. T., & Mitchell, J. K. (1973). *Static Penetration Resistance of Soils*. University of California, Berkeley.

Moavenian, M. H., Nazem, M., Carter, J. P., & Randolph, M. F. (2016). Numerical analysis of penetrometers free-falling into soil with shear strength increasing linearly with depth. *Computers and Geotechnics*, *72*, 57–66.

Nazem, M., Carter, J. P., Airey, D. W., & Chow, S. H. (2012). Dynamic analysis of a smooth penetrometer free-falling into uniform clay. *Géotechnique*, *62*(10), 893–905.

Omidvar, M., Iskander, M., & Bless, S. (2012). Stress-strain behavior of sand at high strain rates. *International Journal of Impact Engineering*, *49*, 192–213.

Phuong, N. T. V, van Tol, A. F., Elkadi, A. S. K., & Rohe, A. (2016). Numerical investigation of pile installation effects in sand using material point method. *Computers and Geotechnics*, *73*, 58–71.

Sabetamal, H., Carter, J. P., & Sloan, S. W. (2018). Pore Pressure Response to Dynamically Installed Penetrometers. *International Journal of Geomechanics*, *18*(7), 1–16.

Stark, N., Hay, A. E., & Trowse, G. (2014). Cost-effective geotechnical and sedimentological early site assessment for ocean renewable energies. *OCEANS ,*2014.